



ELSEVIER

Contents lists available at ScienceDirect

International Journal of Greenhouse Gas Control

journal homepage: www.elsevier.com/locate/ijggc

Seismic amplitude analysis provides new insights into CO₂ plume morphology at the Snøhvit CO₂ injection operation

James C. White^{a,*}, Gareth Williams^b, Andy Chadwick^a^a British Geological Survey, Keyworth, Nottingham, NG12 5GG, UK^b British Geological Survey, Edinburgh, EH9 3LA, UK

ARTICLE INFO

Keywords:

Seismic monitoring
 Snøhvit
 Spectral decomposition
 Time-lapse geophysics

ABSTRACT

CO₂ has been injected at the Snøhvit Field since 2008, with the storage operation split between two distinct injection phases. Until 2011, CO₂ was sequestered in the deeper Tubåen Formation before problems with increasing pressure necessitated moving the injection to the overlying Stø Formation.

A comprehensive time-lapse seismic monitoring programme has been undertaken over the injection site throughout this period. Uniquely, this study examines four separate seismic vintages starting with the 2003 baseline data and ending with the 2012 repeat survey. The 3D seismic reflection data reveal the seismic character of the anomalies imaged in the Tubåen and Stø Formations to be dissimilar. Time domain analysis and spectral decomposition are used to investigate the CO₂ plume morphology in both cases.

The seismic response during the initial phase is complex, showing contributions from both fluid and pressure changes. The majority of the reflectivity is ascribed to a build-up of pore-water pressure in the wider reservoir. Seismic analysis of the second phase reveals a simpler distribution, consistent with a conical plume formed by buoyancy-driven upward advection of CO₂. The thickness of the spreading layer is calculated, and a maximum temporal thickness of 22 ms is derived from both time and frequency analysis. Direct comparison of the two methodologies reveals good agreement over the central parts of the layer where spectral techniques are applicable. Results are then used to determine the total mass of CO₂ in the Stø Formation as 0.51 million tonnes. This is consistent with the true injected mass of 0.55 million tonnes.

1. Introduction

The Snøhvit CO₂ injection operation is located in the central part of the Hammerfest Basin, beneath the Barents Sea offshore northern Norway (Fig. 1(a)). The deeper part of the Hammerfest Basin sedimentary succession is compartmentalised into a series of fault-bounded blocks, typically several kilometres wide, which define the structure in the vicinity of the storage complex.

Two sandstone reservoirs, the Tubåen and Stø Formations, of early to middle Jurassic age, have been used as CO₂ stores. They are buried beneath a thick Upper Jurassic to Quaternary overburden at depths of around 2600 and 2450 m respectively. The Tubåen Formation is a markedly heterogeneous fluvial-deltaic to tidal sandstone around 100 m thick. The overlying Stø reservoir is a shallow-water marine sandstone typically 85 m thick. The sealing Nordmela Formation separates the two reservoirs.

The primary operation at the Snøhvit site is the extraction of natural gas. The gas contains around 6% CO₂ which is separated at a nearshore

processing facility near Hammerfest and returned by pipeline for injection through infrastructure located on the seabed. Water depth is approximately 330 m.

Injection of CO₂ into the Tubåen reservoir commenced in 2008, with just over one million tonnes of CO₂ stored by the time injection ceased in early-2011 (Injection Phase 1). Injection Phase 1 was terminated because of a steady increase in downhole pressure (Fig. 2) (Hansen et al., 2011). Injection into the overlying Stø reservoir began in mid-2011 with about 0.5 million tonnes injected by 2012 (Injection Phase 2). Injection Phase 2 is performing as expected, with no significant increase in downhole pressure (Fig. 2) (Osdal et al., 2013, 2014).

A baseline 3D seismic reflection survey was acquired over the storage site in 2003, prior to injection, with repeat 3D surveys acquired in 2009, 2011 and 2012 (Fig. 2). A downhole pressure gauge is installed in the injection well at a depth of ~1800 m, some 800 m above the Tubåen reservoir and ~600 m above the Stø Formation.

Possible causes of the rapid initial pressure increase in Injection

* Corresponding author.

E-mail addresses: jame3@bgs.ac.uk (J.C. White), gwil@bgs.ac.uk (G. Williams).<https://doi.org/10.1016/j.ijggc.2018.05.024>

Received 5 January 2018; Received in revised form 17 May 2018; Accepted 30 May 2018

Available online 13 July 2018

1750-5836/ © 2018 British Geological Survey © UKRI 2018. Published by Elsevier Ltd. This is an open access article under the CC BY license (<http://creativecommons.org/licenses/by/4.0/>).

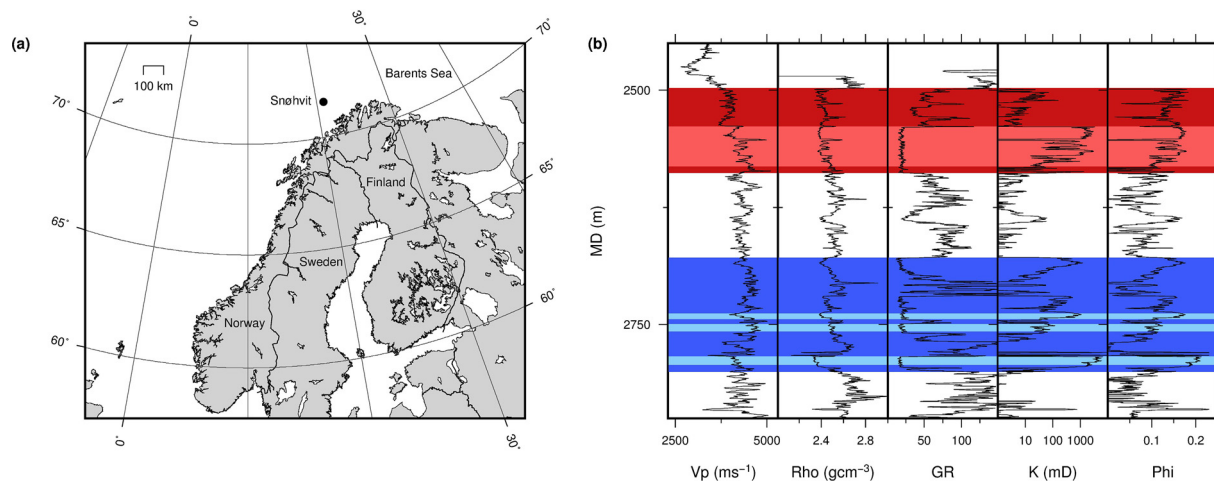


Fig. 1. (a) Location of Snøhvit CO₂ operation in the Barents Sea, Norway. (b) Sonic, density, gamma ray, permeability and porosity logs from the CO₂ injection well. The Stø Formation (shown in red) is separated from the Tubåen Formation (displayed in blue) by the Nordmela Formation. Injection perforations for Injection Phase 1 are shaded light blue. The single perforation for Injection Phase 2 is shaded light red. (For interpretation of the references to colour in this figure legend, the reader is referred to the web version of this article.)

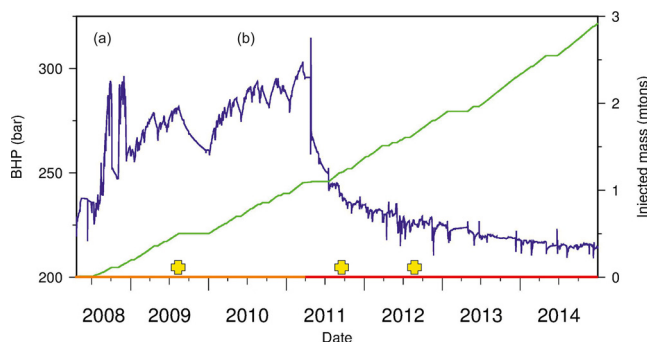


Fig. 2. Downhole pressure during CO₂ injection at Snøhvit from a pressure gauge located at ~1800 m depth is displayed in blue. Cumulative injected mass is shown in green. Seismic survey acquisition dates are marked with a yellow cross. The change from Tubåen to Stø injection is marked by the change from orange to red on the x-axis. (For interpretation of the references to colour in this figure legend, the reader is referred to the web version of this article.)

Phase 1 have been the topic of discussion. Wireline logs through Tubåen Formation show that the perforated zones are separated by shaly intervals in the vicinity of the injection well (Fig. 1). These could act as obstacles to vertical advection of CO₂. In addition, it is likely that major compartmentalising faults imaged on seismic data (see below) form low permeability barriers in the Tubåen Formation, occluding horizontal fluid transport and resulting in pressure compartmentalisation. Hansen et al. (2013) have highlighted a NW-SE trending channel in the Tubåen Formation, of higher permeability and porosity than the bulk of the reservoir, which is intersected by the injection well. As such, the drilled region may not be entirely representative of the surrounding geology. Osdal et al. (2014) ascribed the rapid pressure increase to low reservoir permeability close to the near-well zone, whereas Grude et al. (2013) postulated a significant pore pressure increase across the entire fault-block, based on time-lapse 3D seismic data inverted for both pressure and saturation changes. White et al. (2015) used 3D seismic data acquired in 2009 during the Tubåen injection phase to discriminate between saturation and pressure changes based on the spectral response of the seismic anomaly. They concluded that fluid substitution effects caused the near-well seismic difference signal, whereas the far-field time-lapse response reflected increased reservoir fluid pressure.

This paper reviews geophysical monitoring undertaken at Snøhvit to understand and image the changes in the subsurface generated as a

consequence of CO₂ injection. Subsequently, we compare the observed and markedly different seismic responses from the two injection phases and interpret these in terms of plume morphology and pressure evolution in each reservoir. Furthermore, amplitude mapping and spectral analysis have been used to quantify the thickness of the CO₂ layer imaged in the Stø Formation, with a view to estimating the mass of CO₂ trapped in the reservoir.

2. Monitoring at Snøhvit

The monitoring programme at Snøhvit combines continuous downhole pressure monitoring plus 3D time-lapse seismic imaging conducted at intervals of around one to two years.

2.1. Downhole pressure

Smoothed bottom-hole pressures for the CO₂ injector well show a number of features (Fig. 2). Rapid and large initial pressure increases, highlighted by (a) in Fig. 2, were associated with near-wellbore salt precipitation and flushing with a monoethylene glycol (MEG) solvent corrected this issue (Hansen et al., 2013). A longer-term pressure increase (b) was also observed over injection phase 1. This involved pressures rising over a period of three years from an initial near-hydrostatic 300 bar (estimated in Tubåen Formation from pressure gauge data) to about 370 bar, only ~20 bar beneath the estimated fracture pressure. A number of short-lived pressure reductions during this period correspond to spells when injection was suspended. Injection Phase 1 was terminated due to the steady pressure increase, and the well was plugged above the perforations in the Tubåen Formation. Fluid flow modelling of the pressure response to CO₂ injection/suspension into the Tubåen Formation suggests that the reservoir is compartmentalised, with a relatively small, connected pore volume (Shi et al., 2013).

Injection phase 2 was initiated in summer 2011, injecting CO₂ temporarily into the Stø Formation in anticipation of a new CO₂ injector. Following the plugging of the well above the lower perforations, downhole pressures reflect fluid flow in the Stø Formation, with the initially elevated near-wellbore pressures gradually decreasing to a steady-state, near-hydrostatic pressure of around 270 bar in the Stø Formation. This suggests that any potential pressure increase in the Stø Formation due to CO₂ injection rapidly dissipates into a larger aquifer. A new injector was drilled in the autumn of 2016, injecting into the Stø Formation in an adjacent fault block and minimising risk of future migration into the natural gas pool.

Table 1
Details of the 3D time-lapse seismic surveys acquired over the Snøhvit CO₂ storage site analysed in this paper.

Year of survey	Extent of survey	Mass injected into Tubåen Fm. (mT)	Mass injected into Stø Fm. (mT)	Comments
2003	8.25 × 9.63 km	0	0	Baseline survey for Tubåen injection phase.
2009	7.71 × 9.63 km	0.5	0	First repeat survey for Tubåen injection phase. Baseline survey for Stø injection phase.
2011	3.15 × 8.75 km	1.05	0.13	Significantly smaller spatial extent than other surveys.
2012	8.25 × 10.2 km	1.05	0.55	Final survey available to this study.

2.2. Time-lapse seismic data

3D time-lapse seismic surveys were acquired at Snøhvit in 2003, 2009, 2011 and 2012 (Fig. 2; Table 1).

Seismic data processing was undertaken on two separate occasions making quantitative comparisons between all the surveys problematic. At the outset, the 2003 pre-injection survey formed the baseline for the first repeat survey in 2009. Then, following acquisition of later data vintages and revision of the time-lapse processing flow, the 2009 survey became the baseline survey for the subsequent (2011 and 2012) surveys after the second processing iteration. This is a consequence of the primary focus shifting to imaging the overlying Stø Formation. The change in vintage of the baseline survey ensures that the improvements in marine 3D seismic acquisition and processing that took place between 2003 and 2009, and result in enhanced imaging of the reservoir, are fully exploited. However, a complicating factor for interpreting time-lapse changes is that CO₂ was already present in the subsurface when the 2009 dataset was acquired, and injection into both the Tubåen and Stø Formations occurred between this and subsequent surveys (Table 1).

Seismic lines from the 2003 and 2009 surveys centred on the injection point show the general geological structure of the Snøhvit field (Fig. 3). The Stø Formation is not well imaged on the seismic data, but the reflection from the top of the overlying Fuglen Formation, which sits directly above the Stø Formation acts as a regional seismic marker. The top of the Tubåen Formation is also not well imaged, but the base Tubåen Formation is imaged across the survey area, albeit with reflection amplitudes significantly reduced at the eastern edge of the survey where the reservoir is located beneath a gas accumulation in the overburden. A set of E-W trending normal faults, clearly visible on the N-S seismic lines, cut the reservoir layers into a series of fault-blocks.

The seismic anomaly generated by the CO₂ is not immediately obvious on the repeat seismic surveys as relative amplitude changes are quite small, proportionally less for example than those produced after CO₂ emplacement at some other large storage projects e.g. Sleipner (Chadwick et al., 2016; Chadwick et al., 2004; White et al., 2018). The difference data however do clearly show the acoustic response of the injected CO₂ (Fig. 3) in both the Tubåen and (post-2009) the Stø reservoirs. It is noteworthy that the 2011 and 2012 difference data contain reflectivity from the CO₂ trapped in the Stø, plus the effects of

velocity pushdown on the deeper CO₂ related reflectivity in the Tubåen.

Although not a topic for this paper, an important observation from the data is that no upward leakage is observed during either phase of injection suggesting secure containment of CO₂.

3. Time-lapse seismic response in the Tubåen Formation

The Tubåen Formation is stratigraphically complex, consisting principally of deltaic sediments with evidence of both fluvial and marine influence. In addition, variability in porosity and permeability observed on well logs (Fig. 1) might be a consequence of highly variable cementation during burial. The clean sands of the Tubåen Formation (Grude et al., 2013) are interspersed with thin shale layers that are likely to hinder vertical flow of injected CO₂. Maldal and Tappel (2004) demonstrated that correlation of these baffles between adjacent exploration wells is difficult; implying the sand and shale distribution is irregular and impersistent and that pressure communication throughout the Tubåen Formation is likely.

During Injection Phase 1 CO₂ was injected through three perforation intervals, with over 80% of the CO₂ believed to have entered through the lower perforation close to the base of the Tubåen Formation (Hansen et al., 2011). The injection well has been interpreted as intersecting a high permeability clean sandstone channel, which trends NW-SE (Hansen et al., 2013).

3.1. Seismic changes between 2003 and 2009

Fig. 4 shows absolute seismic amplitude plots extracted on the base Tubåen Formation reflection for the four seismic surveys acquired at Snøhvit (Table 1). Amplitude difference data highlight the spatial extent of the anomaly in the area surrounding the injection point. An amplitude anomaly covering an area of over 5 km² is observed on the 2009–2003 difference plot (Fig. 4c). The anomaly has two components: a narrow NW-SE linear zone of high amplitude centred on the injection point, likely corresponding to a sandstone channel, and a more widespread zone of moderate to low amplitude displaying a mottled lateral variability. If the anomaly were to be caused entirely by fluid substitution it would require a layer of CO₂ at least 1-m-thick across the entire extent of the anomaly, with thicker accumulations in the vicinity of the injection point, in the narrow linear zone. This indicates rapid

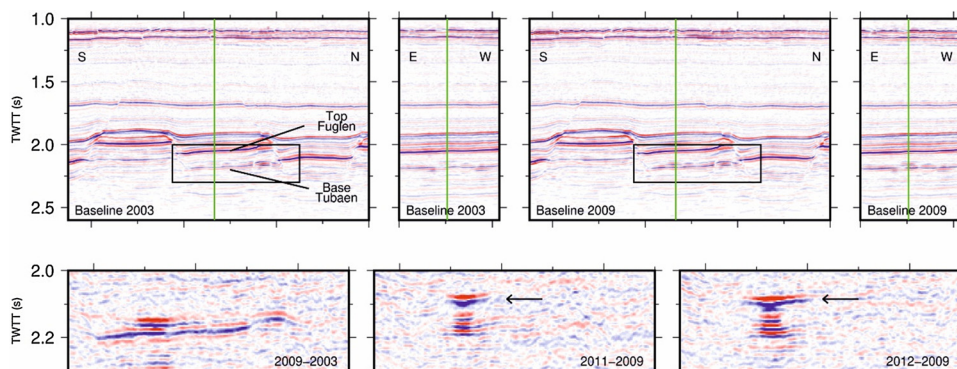


Fig. 3. Seismic lines from the first baseline (2003) and the second baseline (2009) surveys highlighting the geological structure at Snøhvit (top). Difference data shows changes between 2003 and 2009, and subsequent to 2009 (bottom). Green lines delineate the intersection between the N-S and E-W lines. Black boxes show the location of the difference panels. Arrows point to the Stø anomaly, to differentiate from the deeper time-shifted Tubåen reflectivity. (For interpretation of the references to colour in this figure legend, the reader is referred to the web version of this article.)

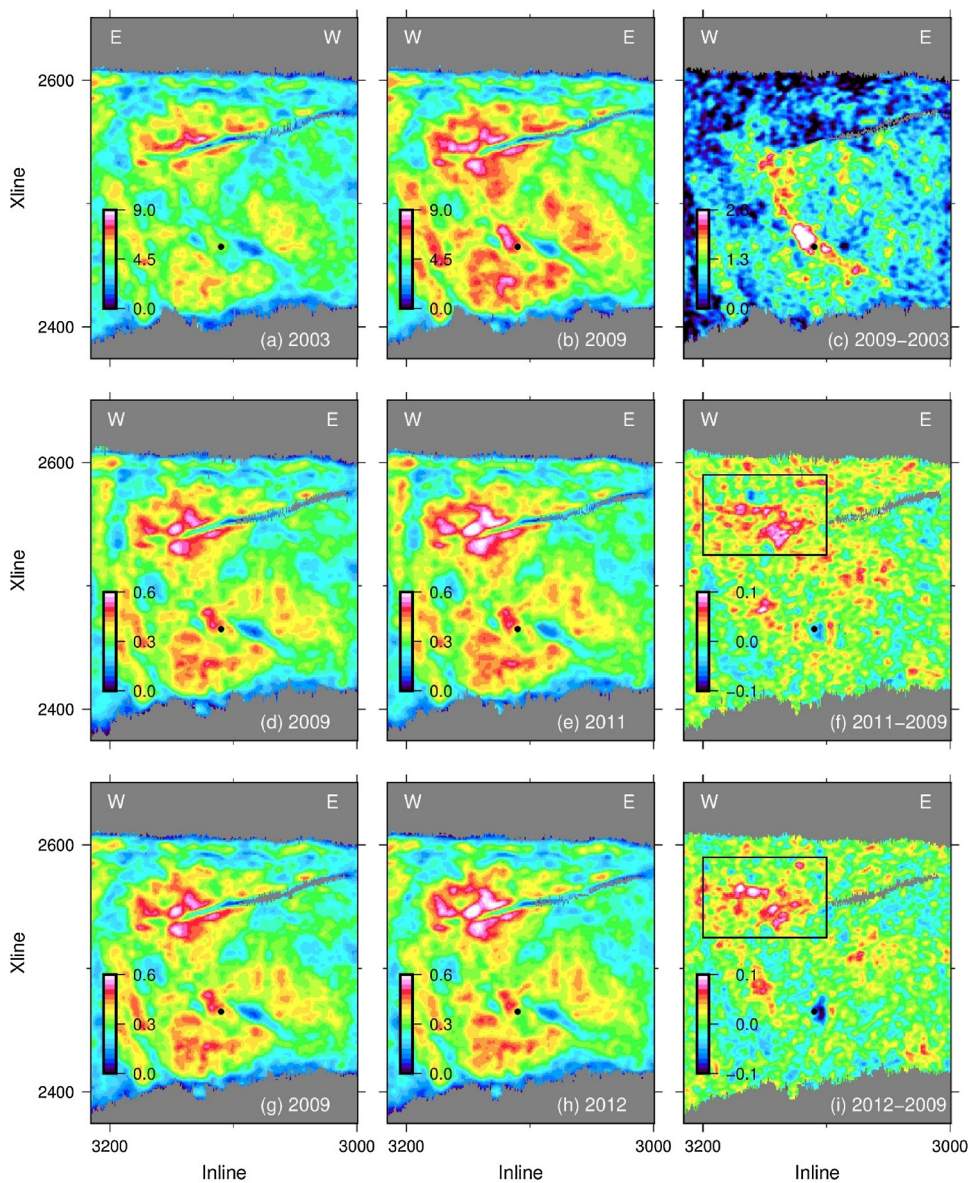


Fig. 4. Reflection amplitudes for the base Tubåen extracted from the 2003, 2009, 2011 and 2012 seismic surveys acquired at Snøhvit. Each panel has an area of approximately 9 km². Inline and Xline spacing for the 3D surveys was 12.5 m. The right-hand panels, (c), (f) and (i), show the difference between the baseline, (a), (d) and (g), and subsequent repeat, (b), (e) and (h), data. The injection point is shown with a black dot. The area delineated by the black box is discussed in detail below. Note the change in the seismic amplitude colour-scale between the top and subsequent rows, a consequence of the two iterations of processing. This is emphasised by the difference between (b) and (d) which show the same data processed at different times.

and rather uniform lateral migration of the CO₂ outside of the permeable channel. This is intuitively rather unlikely given the permeability and complex architecture of the reservoir and is not consistent with published flow simulations of plume evolution (e.g. Hansen et al., 2013; Shi et al., 2013).

An increase in pore-pressure acts to reduce effective stress in the formation causing a decrease in P-wave velocity which, if sufficiently large, can generate a detectable signal in the seismic difference data. Fluid injection into reservoirs with a limited connected pore volume has been shown to generate seismic amplitude responses that can be directly attributed to both pressure and saturation change (Angelov et al., 2004; Landrø, 2001). Grude et al. (2014) and White et al. (2015) have both proposed that the seismic response in the Tubåen reservoir represents the combined effects of both pressure and fluid saturation changes.

White et al. (2015) utilised spectral decomposition techniques to discriminate between fluid substitution and pressure changes. A clear spatial separation was observed between areas of low and high frequency tuning (Fig. 5). This reflects the fact that the pressure anomaly propagates over a greater vertical extent of the reservoir than the CO₂ plume which is restricted to the lowest sandstone unit in the Tubåen Formation, the former characterised by tuning at low seismic

frequencies. Their results showed good agreement with previous attempts to differentiate between CO₂ saturation changes and pressure increases in the Tubåen Formation using amplitude vs offset (AVO) analysis (Hansen et al., 2011; Grude et al., 2013). The 2003 and 2009 data therefore suggest that a build-up of pore-water pressure in the wider reservoir was responsible for most of the observed difference signal, with a smaller zone of high saturation CO₂, located close to the injection point. Within this zone most of the CO₂ is likely to be trapped beneath the deepest intra-Tubåen mudstone layer.

It is notable that the wider, pressure induced difference anomaly (Fig. 5a) is largely terminated by the faults, indicating that they are forming barriers to water flow and effectively compartmentalising the reservoir.

3.2. Seismic changes between 2009 (new baseline) and 2012

Injection into the Tubåen Formation ceased in the spring of 2011, with a total of 1.05 Mt of CO₂ injected by the time the 2011 monitor survey was acquired. It is clear (Fig. 4f) that the amplitude anomaly directly surrounding the injection point had diminished slightly by 2011 and more markedly by 2012 (Fig. 4i). This is consistent with migration of CO₂ away from the near well zone following cessation of

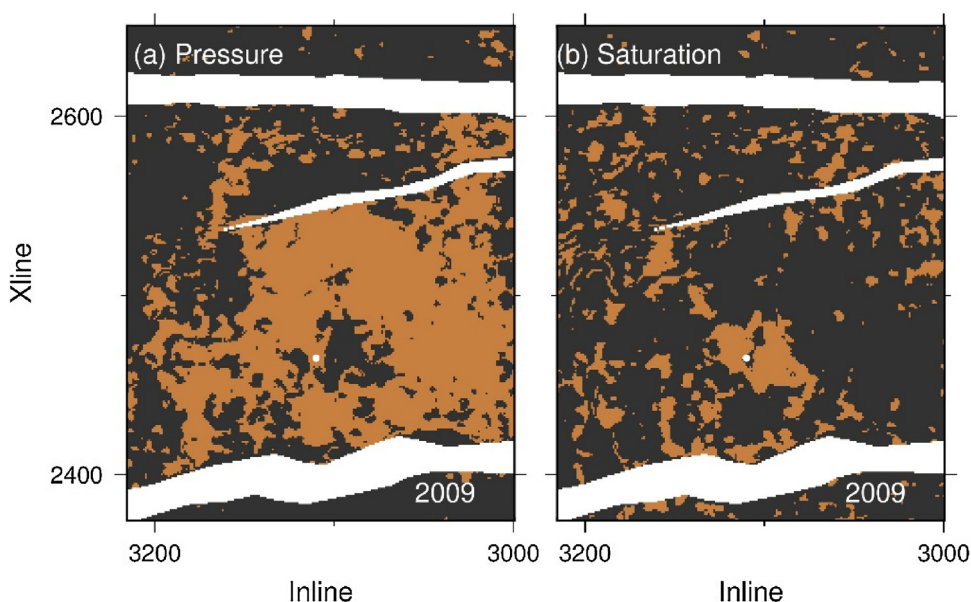


Fig. 5. Discrimination between pressure and saturation changes in the Tubåen using spectral decomposition, after White et al. (2015). Orange region reveals extent of anomaly. The white polygons represent mapped faults in the Tubåen. The white dot shows the location of the injection well. Inline and Xline spacing for the 3D surveys was 12.5 m. (For interpretation of the references to colour in this figure legend, the reader is referred to the web version of this article.)

injection, although it could also be caused by a change in fluid pressure or attenuation of the seismic signal as it passes through the CO₂ accumulating in the overlying Stø Formation (see below). The anomaly at the northern end of the high permeability channel (marked by the black box in Fig. 4) continued to grow spatially through 2011 and 2012 and increase in amplitude, implying continued build-up of CO₂ here. This is consistent with the CO₂ migrating up-dip to the north-west in the Tubåen Formation, largely driven by buoyancy following the cessation of injection. It is important to note that there is no significant decrease in the more widespread difference amplitudes across the fault-block suggesting that the induced pressure increase had yet to dissipate significantly.

4. Results – Time-lapse seismic response in the Stø Formation

Injection into the Tubåen Formation ceased in April 2011, with a new perforation opened in the overlying Stø Formation. This reservoir lies at a depth of around 2450 m and is separated from the Tubåen Formation by the low permeability Nordmela Formation. It comprises predominantly shallow marine sediments and is markedly less stratigraphically heterogeneous than the Tubåen Formation (Worsley et al., 1988). Well logs (Fig. 1) show that the Stø Formation has a porosity of up to 20% and permeabilities in the range 500–700 mD. By the time of the 2012 seismic survey Injection Phase 2 had injected around 0.55 mT of CO₂ through a single perforation.

Seismic data suggest that the CO₂ spreads radially out from the wellbore to form a conical plume (Fig. 3). Osdal et al. (2013) state that because of the homogeneous nature of the reservoir, good lateral and vertical hydraulic communication in the Stø Formation is expected, a supposition supported by the pressure data (Fig. 2), which are consistent with an open permeable reservoir. Note that phase 2 of the injection consequently brought the CO₂ sequestration operation into pressure communication with the gas production wells. Minimal pressure build up was observed as a consequence of CO₂ injection yet the drilling of a new injector has now moved injection away from the gas zones.

The top and base reflections from the CO₂ layer in the Stø Formation were picked on the 2011 and 2012 seismic difference data (Fig. 3, lower panels), and from these temporal spacing (the time on the seismic trace between the reflections) and reflection amplitudes were extracted and mapped (Fig. 6). Over most of the survey area the CO₂ layer has a constant temporal spacing of approximately 13.5 ms. This represents

the temporal tuning thickness for a seismic wavelet of dominant frequency ~35–40 Hz. In this situation the top and base of the thin layer cannot be individually resolved using conventional time domain analysis and the trough-peak couplet displays a constant temporal offset that is a consequence of the superposition of the two reflections. However, increased temporal spacings, up to more than 20 ms, occur in a central zone around the injection point on both the 2011 and 2012 surveys shows (Fig. 6c,f). Here, explicit imaging of the top and base of the CO₂ layer is achieved and provides the potential for direct measurement of CO₂ temporal thickness.

The seismic amplitudes show a peak response close to the injection point (Fig. 6a–d), but there is a significant degree of spatial mismatch between respective maxima in the measured temporal spacing and measured reflection amplitude (compare Figs. 6d–f). This is investigated further below.

4.1. True temporal layer thicknesses from wedge modelling

In order to analyse the reflection response more closely, a 2D elastic model of a wedge of CO₂ was created (Fig. 7), parameterised with values for the Stø Formation derived from well logs (Fig. 1) allowing direct comparison with the observed data. Fluid substitution was based on a homogeneous Gassmann approximation (Gassmann, 1951) at 80% CO₂ saturation, with CO₂ properties at reservoir temperature and pressure calculated using the Span and Wagner (1996) equation-of-state for pure carbon dioxide.

Synthetic seismic traces were generated using a convolutional modelling scheme. This approach results in a seismic section (Fig. 7b) equivalent to a stacked image. A Ricker wavelet of 40 Hz peak frequency was used in the modelling, the negative and positive reflections correspond to the top and base of the CO₂ layer respectively (Fig. 7b). Reflection amplitudes increase progressively from zero at zero-layer thickness to a maximum at a layer travel-time thickness of 13.5 ms, corresponding to the tuning thickness of the source wavelet. Above this, reflection amplitudes decrease somewhat as the top and base layer reflections separate further. Beneath the tuning thickness, the measured temporal spacing (the time between top and base reflections picked on the seismic data) remains roughly constant at 13.5 ms (Fig. 7c), the same as observed in the Snøhvit data following injection into the Stø Formation (Fig. 6). Above the tuning thickness the temporal spacing increases and can be used to derive the layer thickness (Fig. 7c), with an appropriate correction to convert the measured temporal spacing (blue

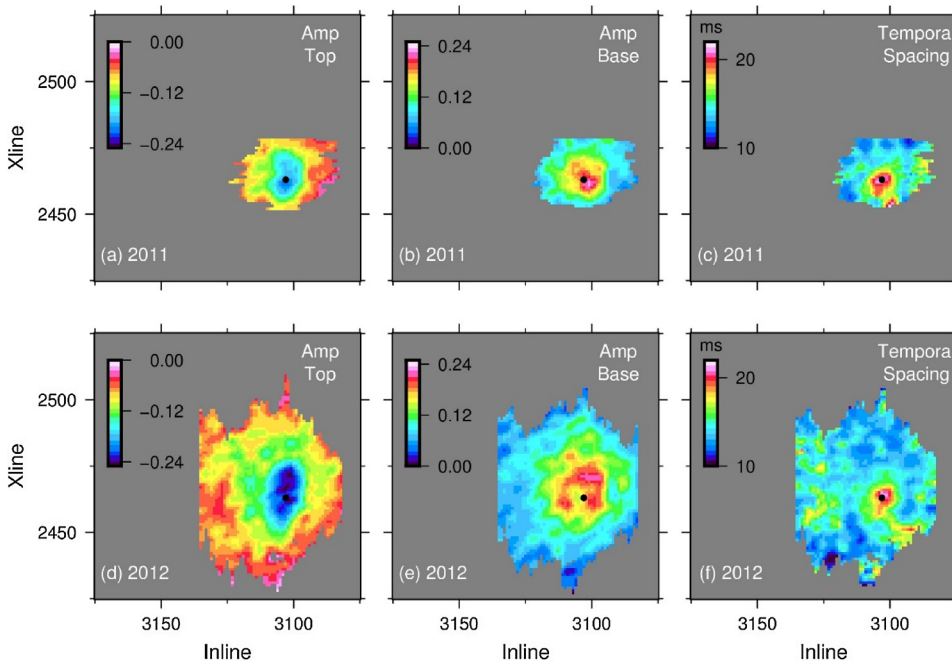


Fig. 6. Time and amplitude seismic analysis of the growing CO₂ layer in the Stø Formation in 2011 and 2012. (a) (b) (d) and (e) display reflection amplitudes from the top and base of the layer. (c) and (f) show the temporal spacing between the two reflections measured in two-way travel time. The Injection point is marked with a black dot. Inline and Xline spacing for the 3D surveys was 12.5 m.

line) to true temporal thickness (purple line).

The insights gained from the wedge model are then used to determine the true temporal thickness of the CO₂ layer in the Stø Formation. Thicknesses are calculated using measured reflection amplitudes beneath the tuning thickness whilst measured temporal spacings are used above it. So, where the temporal spacing exceeds 13.5 ms, a corrected temporal thickness was calculated via a simple polynomial that describes the relationship between the blue and the purple lines in Fig. 7c. Beneath the tuning thickness, the amplitude-thickness relationship from the wedge model was used to estimate the true temporal thickness of the layer. Amplitude relationships between observed and synthetic data are normalised with the peak reflection amplitude in each data set, then used to infer the temporal thickness using the relationship highlighted by the green line in Fig. 7 (c). It is noted that around the tuning thickness (~13.5 ms) two possible temporal thickness values exist for a single amplitude value, one below and one above the tuning thickness. In fact, only the lower temporal thickness is relevant because the higher thickness falls within the area covered by the measured temporal spacing analysis

Fig. 8 displays true temporal layer thicknesses from 2011 and 2012 and these show a roughly radial layer geometry with values increasing smoothly from zero at the layer margins to peaks in excess of 20 ms at the injection point.

4.2. True temporal layer thicknesses from spectral decomposition

In seismic imaging of a layered medium, tuning effects from thin layers preferentially enhance distinct frequency (spectral) components of the incident wave-field. Spectral decomposition can be used to identify preferentially tuned frequencies, which are related directly to layer temporal thickness. Spectral decomposition has been used to improve imaging of complex stratigraphical sequences (Partyka et al., 1999; Chen et al., 2008; Laughlin et al., 2003; McArdle and Ackers, 2012) and characterise thin CO₂ layers at injection sites such as Snøhvit (White et al., 2015), Ketzin (Huang et al., 2015) and Sleipner (Williams and Chadwick, 2012; White et al., 2013; White et al., 2018). Here we demonstrate its efficacy on the wedge model and then apply it to the Snøhvit seismic data. In doing so, we provide a second methodology to verify our plume thickness estimates, increasing confidence in the results if agreement between the methods is observed. Additionally, a

technique to estimate layer thicknesses in the subsurface, applicable to data where distinct reflections from the top and base of the CO₂ layer are difficult to measure, is tested on a real CO₂ storage operation providing a tool for operators to verify storage site conformance.

A CO₂ layer generates a top and base reflection, normally of opposite polarity, which if the layer is sufficiently thin, interfere with each other to produce a tuned wavelet on the seismic trace. The frequency domain impulse response, $G(f)$, of tuned reflections from a thin layer is determined by Marfurt and Kirilin (2001):

$$G(f) = r_1 e^{-2\pi i f t_1} + r_2 e^{-2\pi i f (t_1 + T)} \quad (1)$$

where f is the frequency in Hz, r_1 and r_2 are the reflection coefficients of the top and bottom interface, t_1 is the two-way travel time (s) to the top of the layer and T is the two-way travel-time (temporal) thickness (s), of the thin layer. Optimal tuning occurs (the first spectral peak) where

$$f = 1/(2T) \quad (2)$$

and then at subsequent harmonic modes (2nd, 3rd, etc. spectral peaks) where

$$f = (n + 1/2)/T \quad (3)$$

and n is an odd integer.

A change in the temporal thickness of the causative layer will produce tuning at different frequencies. Once the frequency of the first spectral peak is determined the temporal layer thickness follows directly.

Williams and Chadwick (2012) evaluated a number of spectral windowing methodologies to isolate the response from a short analysis window, concluding that the Smoothed Pseudo Wigner-Ville Distribution (SPWVD) gave the best results. The SPWVD,

$$SPWVD_{x(t,v)} = \int_{-\infty}^{+\infty} h(\tau) \int_{-\infty}^{+\infty} g(x-t)x\left(t + \frac{\tau}{2}\right)x^*\left(t - \frac{\tau}{2}\right) dt e^{-i2\pi\nu\tau} d\tau \quad (4)$$

utilises smoothing functions, $g(x-t)$ and $h(\tau)$, in time and frequency respectively, to remove spurious cross-terms which can reduce the resolution of the algorithm. Here, t is time, τ the lag, ν the frequency and $*$ represents complex conjugation.

Frequencies between 10 and 54 Hz were used for analysis with spectral decomposition, characteristic of the frequency content of the

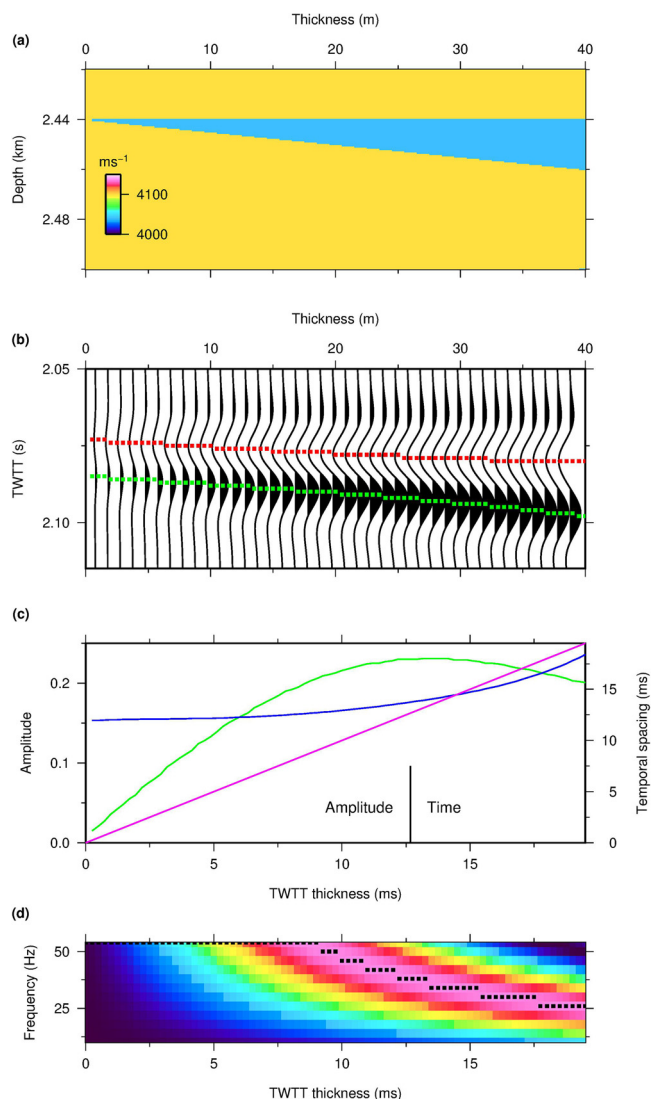


Fig. 7. Synthetic model of a CO₂ wedge spreading within the Stø Formation. (a) P-wave velocity distribution calculated using homogeneous Gassmann fluid substitution. (b) Synthetic seismic data from the wedge model. Red and green dashed lines highlight peak amplitude picks for the top and base reflections respectively. (c) Time domain analysis of the wedge model showing: reflection amplitude from the base of the layer (green line); temporal spacing between the top and base reflections (blue line); 1:1 correlation between true temporal thickness and measured temporal spacing (purple line). (d) Spectral analysis of the wedge model using the SPVVD (see below). Normalised peak frequencies decrease from > 50 Hz in the thinner region to < 30 Hz in the thicker part of the wedge. Black dots show the peak discrete frequency at each trace location. (For interpretation of the references to colour in this figure legend, the reader is referred to the web version of this article.)

Snøhvit seismic data.

4.2.1. Wedge model

The SPVVD was used to generate discrete frequency reflection amplitude cubes for the wedge model, sampled every 4 Hz. In order to remove the band-limited spectral content of the source wavelet the individual single-frequency data cubes are normalised using the spectrum incident on the region of interest. This allows different frequencies to be readily compared. The wedge model shows how the peak frequency tracks layer thickness (Fig. 7d) for layer thicknesses both above and below the tuning thickness. It is clear that the available bandwidth is not sufficient to resolve the layer in the thinnest regions but should work adequately in the thicker parts of the distribution.

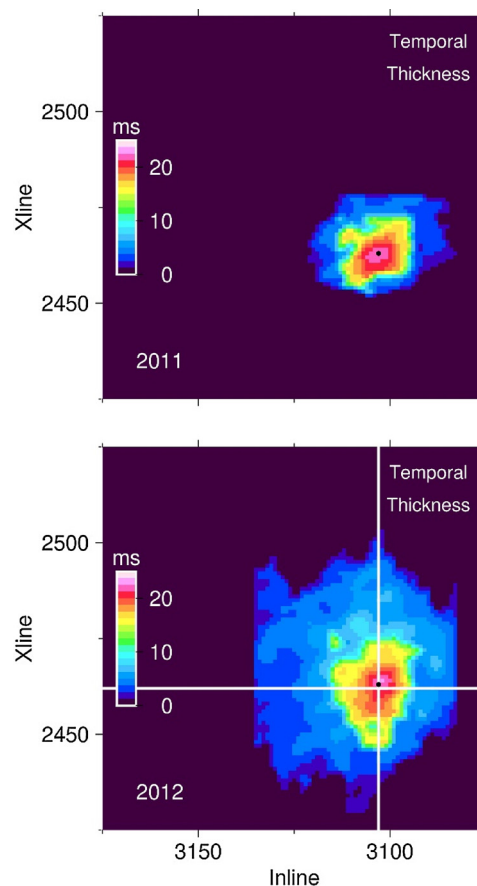


Fig. 8. True temporal thicknesses derived from time and amplitude analysis of the CO₂ layer in the Stø Formation computed from the 2011 and 2012 time-lapse seismic surveys. Black circle marks the injection point. White lines delineate transects shown in Fig. 11. Inline and Xline spacing for the 3D surveys was 12.5 m.

4.2.2. Observed data

Spectral analysis of the observed data indicates that very little energy is present in the highest frequency cubes and that practical resolution of layer thickness falls short of the desired range. Since the tuning thickness corresponds to a peak frequency of 35 Hz, this suggests a broad spectrum with a rapid drop off at higher frequencies for the reflections imaging the Jurassic sequence. Utilising the picked reflection times from the top of the CO₂ layer (Fig. 6), discrete frequency amplitude slices were extracted and gridded. Results for the 2012 dataset show that lower frequencies dominate around the injection point (Fig. 9). This fits with the hypothesis that the layer is thickest in the centre close to the injection well, with progressively higher frequencies tuning farther away from the axial part of the plume. This is consistent with a thinning cone of CO₂ radially reducing in thickness away from the injection point and is in agreement with the time-amplitude analysis (Fig. 8). The overall mapped extent of the seismic anomaly at higher frequencies is also seen to increase. Predictive flow modelling by Osdal et al. (2013) advocated a similar CO₂ distribution in the Stø Formation.

The peak tuning frequency was then determined at each seismic trace location by looping over the sampled frequency range and extracting the frequency band with the highest spectral amplitude. The corresponding temporal thickness was then derived (Eq. ((2)). Temporal thicknesses for the 2011 and 2012 data (Fig. 10) are consistent with true temporal thicknesses derived from the time and amplitude analysis (Fig. 8). The layer is thickest close to the injection point and thins radially toward its margin. Since the bandwidth of the seismic data (at reservoir depth) limits the resolution that can be achieved using spectral decomposition the layer thickness is only resolved to

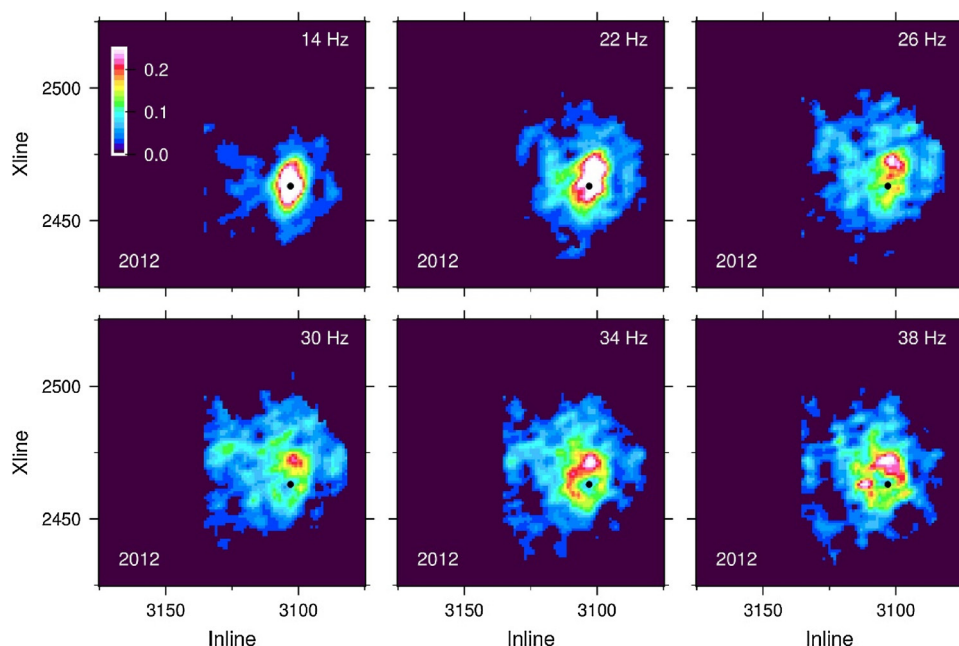


Fig. 9. Normalised discrete frequency reflection amplitudes of the CO₂ layer in the Stø Formation from the 2012 seismic difference data. Inline and Xline spacing for the 3D surveys was 12.5 m.

~11.5 ms. Furthermore, the edge of the anomaly is difficult to determine from the spectral volumes.

4.3. Comparison of the time-amplitude and spectral approaches

True temporal thicknesses calculated from the temporal spacings and amplitudes are compared with results from the spectral decomposition (Fig. 11), via two perpendicular cross-sections extracted from the 2012 temporal thickness maps. Both techniques predict a maximum layer temporal thickness of around 22 ms, with the thickest part of the layer overlying the injection point. This is consistent with a conical plume formed by buoyancy-driven upward advection of CO₂, ponding beneath the impermeable caprock and spreading laterally. It is notable that whilst the layer is considerably larger in 2012 than in 2011, its peak thickness at the injection point is virtually unchanged with a thickness that corresponds to the porous reservoir zone (Fig. 1b) coinciding with the injection perforation. The agreement between maximum calculated layer thickness and the available reservoir zone provides confidence in the analysis.

Spectral decomposition fails to resolve the thickness of the leading edge of the spreading CO₂ layer, which reflects the limited spectral content of the seismic wavelet at reservoir depth (with little energy above 45 Hz). As such, temporal thicknesses beneath 12 ms (shown with dashed blue line in Fig. 11) are removed from the cross-sections. Two distinct peaks, P1 and P2, constitute the principal differences between the two thickness maps. These features coincide with low amplitude edge effects in the data and are unlikely to represent real increases in the thickness of the CO₂.

5. Discussion

Injection into the Tubåen Formation has resulted in two distinctly different reflective components: a linear set of bright reflections trending NW–SE about the injection point and a more extensive diffuse amplitude response across, and roughly limited by, the fault-bounded compartment. Spectral analysis indicates that the former corresponds to thin layering within the CO₂ plume itself, whereas the latter, with lower frequency tuning, is consistent with pressure increase across the whole reservoir thickness. Grude et al. (2014) backed up this

assessment with analytical flow modelling which found that the zone of saturation change would be significantly smaller than the size of the anomaly. Hansen et al. (2013) and White et al. (2015) both published analysis that confirmed these findings.

The Jurassic rocks of the Hammerfest basin have previously been buried up to 1 km deeper than present day, giving rise to increased compaction. Grude et al. (2014) noted the high degree of cementation and significant variation in pore size present in the Tubåen rocks samples available for core analysis. It is believed that outside the higher porosity channel, intersected by the injection well in the deepest unit of the Tubåen Formation, the reservoir is uncondusive to successful long-term CO₂ storage and lacking in the expected permeability and porosity. Additionally, in order to increase injectivity during the early period of the injection operation MEG solvents were utilised to remove precipitated salt from close to the wellbore. A consequence of this approach may be a masking of the seismic signal in the region surrounding the injection perforations. However, it is not feasible that the increased spatial extent of the anomaly can be attributed to this process. In summary, the Tubåen Formation proved to be an unsuitable unit for long term CO₂ storage, yet over 1 mT were successful stored and significant lessons were learnt during the operation. No evidence of leaking CO₂ was observed.

The seismic anomaly in the Stø Formation is simpler, with no evidence of a more spatially extensive pressure-related anomaly. It is consistent with a cone-shaped plume formed by buoyancy-driven upward advection of CO₂, ponding and spreading radially beneath an impermeable topseal. Analytical modelling (Lyle et al., 2005) of radially-symmetric gravity currents shows that layer thickness varies with rate of injection, so this constancy is consistent with the roughly uniform rate of injection. The diffuse amplitude anomaly observed within the Tubåen reservoir is not present in the Stø Formation.

Temporal layer thicknesses can be used to estimate the mass of CO₂ imaged by the seismic data. This is most effective for the Stø Formation where the radially symmetric plume can be more accurately mapped. Assuming a CO₂ saturation of 0.8 (Osdal et al., 2013), a porosity of 17.5% in the Stø Formation (from Fig. 1), a CO₂ density of 712 kg/m³ at in situ conditions (Span and Wagner, 1996) and a velocity of 4025 ms⁻¹ (Gassmann, 1951) for CO₂ saturated reservoir rock, a total mass of 0.51 million tonnes of CO₂, based on the thickness maps in

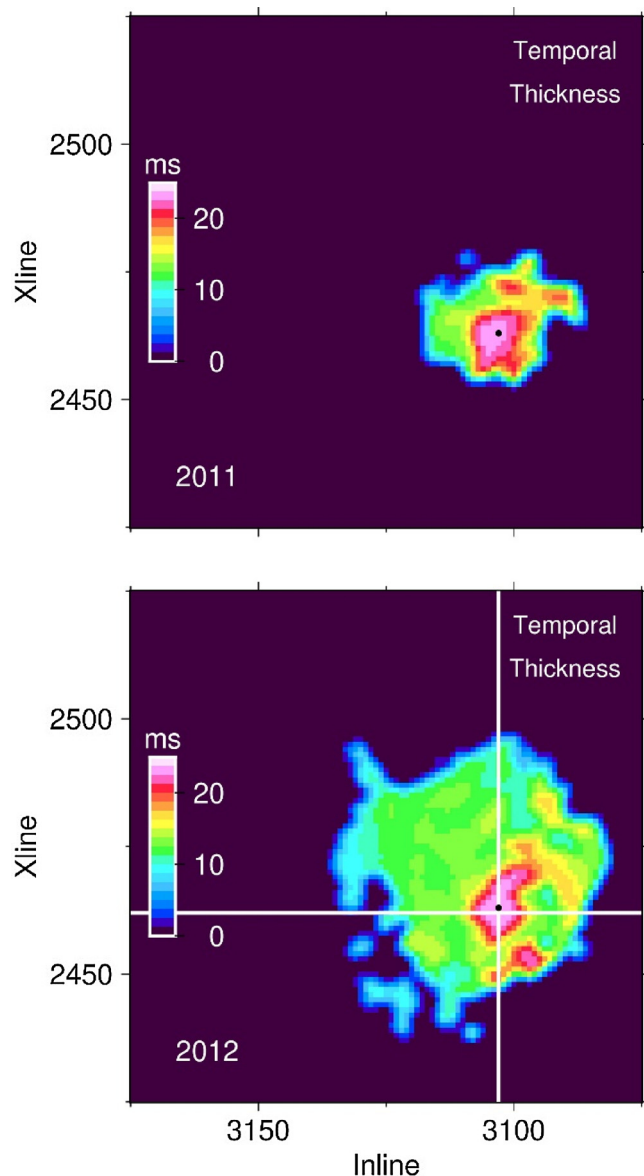


Fig. 10. Peak frequency and the temporal thickness of the Stø Formation CO₂ layer in 2011 (a) and 2012 (b) based on spectral analysis using the SPWVD. The black circle shows the location of the injection well. White lines delineate transects shown in Fig. 11 below. Inline and Xline spacing for the 3D surveys was 12.5 m.

Figs. 8 and 10, is derived. This is consistent with the true injected mass of 0.55 million tonnes measured at the well head, demonstrating the utility of time-lapse seismic monitoring for producing mass balance calculations in the early stages of a CO₂ injection operation. However, significant uncertainties exist in the mass calculation. An average brine saturated velocity, derived over the injection interval from sonic data, is used in the fluid substitution calculation (Gassmann, 1951). Additionally, the porosity shows significant variability in the injection well (Fig. 1b) and may not be entirely representative of the Stø Formation. However, as a first order approximation the mass balance is consistent with the injection history. This assessment of conformance is a key finding, and is not possible for the first phase on injection into the Tubåen Formation.

6. Conclusions

Four time-lapse 3D seismic surveys acquired over the Snøhvit CO₂

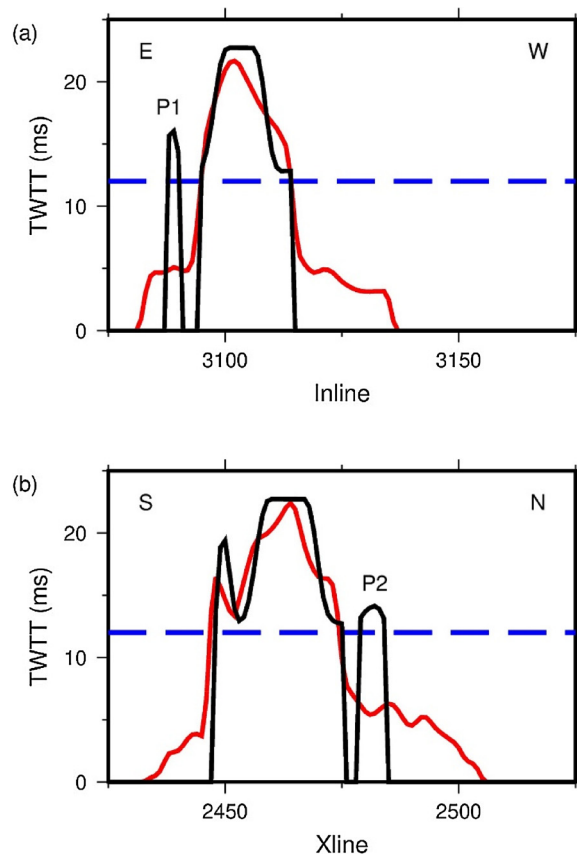


Fig. 11. Plot showing temporal thickness estimates for the Stø Formation CO₂ layer derived using time and amplitude analysis (red curve) and spectral decomposition (black curve). (a) East-west profile; (b) N-S profile. Transect locations are given in Figs. 8 and 10. Peaks labelled P1 and P2 are discussed in text. Dashed blue line shows approximate limit of resolution for spectral decomposition. (For interpretation of the references to colour in this figure legend, the reader is referred to the web version of this article.)

injection operation have been used to estimate the distribution of CO₂ in the reservoir, based on seismic mapping and amplitude analysis. The seismic character of the amplitude anomalies imaged in the Tubåen and Stø Formations differ in both magnitude and spatial extent. The former is geometrically complex with evidence of both fluid saturation and pressure effects. The latter is simpler with radial geometry and suggestive of relatively unimpeded flow and spread of CO₂ in a simple reservoir.

For the Stø reservoir the time-lapse data have been used to test two methodologies for calculating the thickness of the spreading layer and by extension the mass of CO₂ in the reservoir. The results from both techniques are consistent with a CO₂ layer that thins radially away from the injection point. Mass balance calculations based on the seismic data resulted in a total mass of 0.51 million tonnes of CO₂ in the Stø Formation, a good first order match to the known injected mass of 0.55 million tonnes.

Acknowledgements

Statoil ASA and the Snøhvit licence partners Petoro AS, Total E&P Norge AS, Engie E&P Norge AS and DEA Norge AS are thanked for permission to publish this paper. This publication has been produced with support from the BIGCCS Centre, performed under the Norwegian research program Centres for Environment-friendly Energy Research (FME) and from the DiSECCS project (Grant EP/K035878/1) funded by the UK Engineering and Physical Sciences Research Council (EPSRC). JCW, GW and RAC publish with permission of the Executive Director,

British Geological Survey (NERC).

References

- Angelov, P., Spetzler, J., Wapenaar, K., 2004. Pore pressure and water saturation variations: modification of Landrø's AVO approach. SEG Technical Program Extended Abstracts. pp. 2279–2282.
- Chadwick, R.A., Arts, R., Eiken, O., Kirby, G., Lindeberg, E., Zweigel, P., 2004. 4D seismic imaging of an injected CO₂ bubble at the Sleipner Field, central North Sea. In: Davies, R.J., Cartwright, J.A., Stewart, S.A., Lappin, M., Underhill, J.R. (Eds.), 3-D Seismic Technology: Application to the Exploitation of Sedimentary Basins, vol. 29. Geological Society, London. Memoir, pp. 305–314.
- Chadwick, R.A., Williams, G.A., White, J.C., 2016. High-resolution imaging and characterization of a CO₂ layer at the Sleipner CO₂ storage operation, North Sea using time-lapse seismics. *First Break* 34 (2), 77–85 (February).
- Chen, G., Matteucci, G., Fahmy, B., Finn, C., 2008. Spectral-decomposition response to reservoir fluids from a deepwater West Africa reservoir. *Geophysics* 73 (6), C23–30.
- Gassmann, F., 1951. Über die Elastizität poröser Medien *Vierteljahrsschrift der Naturforschenden Gesellschaft in Zürich* 96. pp. 1–23.
- Grude, S., Landrø, M., Osdal, B., 2013. Time-lapse pressure-saturation discrimination for CO₂ storage at the Snøhvit field. *Int. J. Greenh. Gas Control* 19, 369–378.
- Grude, S., Landrø, M., White, J.C., Torsæter, O., 2014. CO₂ saturation and thickness predictions in the Tubåen Fm., Snøhvit field, from analytical solution and time-lapse seismic data. *Int. J. Greenh. Gas Control* 29, 248–255. <https://doi.org/10.1016/j.ijggc.2014.08.011>.
- Hansen, O., Eiken, O., Ostmo, S., Inge Johansen, R., 2011. Monitoring CO₂ injection into a fluvial brine-filled sandstone formation at the Snøhvit field. In: Barents Sea SEG Annual Meeting. San Antonio.
- Hansen, O., Gilding, D., Nazarian, B., Osdal, B., Ringrose, P., Kristoffersen, J.-B., Eiken, O., Hansen, H., 2013. Snøhvit: the history of injecting and storing 1 Mt CO₂ in the fluvial Tubåen Fm. *Energy Procedia* 37, 3565–3573.
- Huang, F., Juhlin, C., Han, L., Kempka, T., Norden, B., Luth, S., Zhang, F., 2015. Application of seismic complex decomposition on thin layer detection of the CO₂ plume at Ketzin, Germany. In: SEG Annual Meeting 2015. New Orleans. pp. 5477–5482.
- Landrø, M., 2001. Discrimination between pressure and fluid saturation changes from time-lapse seismic data. *Geophysics* 66, 836–844.
- Laughlin, K., Garossino, P., Partyka, G., 2003. Spectral decomposition for seismic stratigraphic patterns. *Search Discovery* 4 (article 40096).
- Lyle, S., Huppert, H.E., Hallworth, M., Bickle, M., Chadwick, A., 2005. Axisymmetric gravity currents in a porous media. *J. Fluid Mech.* 543, 293–302.
- Maldal, T., Tappel, I.M., 2004. CO₂ underground storage for Snøhvit gas field development. *Energy* 29, 1403–1411.
- Marfurt, K.J., Kirlin, R.L., 2001. Narrow-band spectral analysis and thin bed tuning. *Geophysics* 66 (4), 1274–1283.
- McArdle, N.J., Ackers, M.A., 2012. Understanding seismic thin-bed responses using frequency decomposition and RGB blending. *First Break* 30, 57–65.
- Osdal, B., Zadeh, H.M., Johansen, S., Gilding, D., 2013. CO₂ saturation and thickness prediction from 4D seismic data at the Snøhvit field. In: 75th EAGE Conference and Exhibition. London.
- Osdal, B., Zadeh, H.M., Johansen, S., Gonzalez, R.R., Waerum, G.O., 2014. Snøhvit CO₂ monitoring using well pressure measurement and 4D seismic. In: Fourth EAGE CO₂ Geological Storage Workshop. Stavanger.
- Partyka, G., Grigley, J., Lopez, J., 1999. Interpretational applications of spectral decomposition in reservoir characterization. *Leading Edge* 18, 353–360.
- Shi, J.-Q., Imrie, C., Sinayus, C., Duracan, S., Korre, A., Eiken, O., 2013. Snøhvit CO₂ storage project: assessment of CO₂ injection performance through history matching of the injection well pressure over a 32-months period. *Energy Procedia* 37, 3267–3274.
- Span, R., Wagner, W., 1996. A new equation-of-state for carbon dioxide covering the fluid region from the triple-point temperature to 1100 K at pressures up to 800 MPa. *J. Phys. Chem. Ref. Data* 25, 1509–1596.
- White, J.C., Williams, G.A., Chadwick, R.A., 2013. Thin layer detectability in a growing CO₂ plume: testing the limits of time-lapse seismic resolution. *Energy Procedia* 37, 4356–4365.
- White, J.C., Williams, G.A., Grude, S., Chadwick, R.A., 2015. Utilizing spectral decomposition to determine the distribution of injected CO₂ at the Snøhvit Field. *Geophys. Prospect.* 63 (5), 1213–1223. <https://doi.org/10.1111/1365-2478.12217>.
- White, J.C., Williams, G.A., Chadwick, R.A., Furre, A.-K., Kiaer, A., 2018. Sleipner: the ongoing challenge to determine the thickness of a thin CO₂ layer. *Int. J. Greenh. Gas Control* 69, 81–95.
- Williams, G., Chadwick, A., 2012. Quantitative seismic analysis of a thin layer of CO₂ in the Sleipner injection plume. *Geophysics* 77 (6), R245–R256.
- Worsley, D., Johansen, R., Kristensen, S.E., 1988. The mesozoic and cenozoic succession of Tromsøflaket. In: Dalland, A., Worsley, D., Ofstad, K. (Eds.), A Lithostratigraphic Scheme for the Mesozoic and Cenozoic Succession Offshore Mid and Northern Norway. Norwegian Petroleum Directorate Bulletin No. 4, pp. 42–65.